Journal of Sound and Vibration 414 (2018) 61–80

Contents lists available at ScienceDirect

Journal of Sound and Vibration

journal homepage: www.elsevier.com/locate/jsvi

# Characterizing human activity induced impulse and slip-pulse excitations through structural vibration

Shijia Pan [a, *], Mostafa Mirshekari [b], Jonathon Fagert [b], Ceferino Gabriel Ramirez [a], Albert Jin Chung [a], Chih Chi Hu [a], John Paul Shen [a], Pei Zhang [a], Hae Young Noh [b]

[a] Carnegie Mellon University, Electrical and Computer Engineering, USA
[b] Carnegie Mellon University, Civil and Environmental Engineering, USA

ARTICLE INFO

*Article history:*
Received 14 March 2017
Received in revised form 29 August 2017
Accepted 22 October 2017
Available online 13 November 2017

*Keywords:*
Structural vibration
Wave propagation
Attenuation
Dispersion
Excitation tracking

ABSTRACT

Many human activities induce excitations on ambient structures with various objects, causing the structures to vibrate. Accurate vibration excitation source detection and characterization enable human activity information inference, hence allowing human activity monitoring for various smart building applications. By utilizing structural vibrations, we can achieve sparse and non-intrusive sensing, unlike pressure- and vision-based methods. Many approaches have been presented on vibration-based source characterization, and they often either focus on one excitation type or have limited performance due to the dispersion and attenuation effects of the structures. In this paper, we present our method to characterize two main types of excitations induced by human activities (impulse and slip-pulse) on multiple structures. By understanding the physical properties of waves and their propagation, the system can achieve accurate excitation tracking on different structures without large-scale labeled training data. Specifically, our algorithm takes properties of surface waves generated by impulse and of body waves generated by slip-pulse into account to handle the dispersion and attenuation effects when different types of excitations happen on various structures. We then evaluate the algorithm through multiple scenarios. Our method achieves up to a six times improvement in impulse localization accuracy and a three times improvement in slip-pulse trajectory length estimation compared to existing methods that do not take wave properties into account.


## 1. Introduction

Human activities induce excitations on the ambient structure (e.g., floors, walls, tables) when performing activities. Characterizing them, especially tracking the source location of the excitation, enables further inference of the human activity information. This activity information can be used in many smart building applications, such as child/patient monitoring, customer behavior analysis, and ubiquitous user input. This structural vibration-based sensing, compared to other methods including vision-, RF-, mobile-, acoustic-, and load-based sensing, enables sparse and non-intrusive sensing on people [1–6]. More detailed comparison between our structural vibration based methods and other sensing approaches can be found in

* Corresponding author.
*E-mail address:* shijiapan@cmu.edu (S. Pan).

https://doi.org/10.1016/j.jsv.2017.10.034
0022-460X/

Section 8.1. These excitations mainly fall into two categories: impact induced impulse excitations (such as footstep, object dropping, door closing, tapping) and friction induced slip-pulse excitations (such as drag a chair, swipe on a surface) [7]. The challenges for vibration based excitation sources tracking include 1) the variance of excitation types and 2) the dispersive nature of the structure materials [8].

Many methods have been presented to track human activity induced excitation through structural vibrations. In particular, works focus on the trajectory estimation of the human induced excitation on the wall by recognizing the specific vibration signal pattern that linked to the trajectory of the excitation [9,10]. These approaches are based on the repetition of the trajectory caused signal pattern, therefore requiring large-scale training data to establish such a relationship. Pham et al. track the human induced excitation sources directly, which is sensitive to medium variation [11–13]. Works have also been done on localizing the human induced excitation such as footsteps and heartbeats [14–16] by taking wave properties into account to handle the dispersive structures. However, these works focus on particular applications.

In this paper, we present our robust structural vibration sensing system that enables various types of human induced excitations (impulse and slip-pulse) tracking under multiple structural conditions. To address the challenges for vibration based excitation sources tracking and achieve high tracking accuracy, we first study the wave properties of different types of excitations to understand the dispersion, propagation and attenuation of impulse and slip-pulse signals. Then we utilize our understanding on wave dispersion, propagation and attenuation for impact-induced impulse and friction-induced slip-pulse to design the algorithm that can obtain accurate Time Difference of Arrival (TDoA) estimations despite these effects. Finally, we use multilateration to calculate locations of the excitation sources and hence achieve tracking. To validate our method, we performed a series of experiments that evaluate the system by computing the accuracy of locating various types of excitation sources with different structural characteristics. The main contributions of this paper are:

- We study the wave properties of human-induced impulse and slip-pulse excitation in structures to enable vibration-based non-intrusive human activity characterization.
- We present our characterization algorithm that reacts to each excitation based on the analytic models of different waves to resolve dispersion and reflection effects and achieve accurate tracking on various structures.
- We characterize and evaluate our method through structures of various materials and sizes with different impulse and slip-pulse excitations for multiple applications.

The rest of the paper is structured as follows: First of all, we provide the background knowledge that supports our work in Section 2. Next, we present the sensing system and explain the characterization of different excitations in Section 3 followed by the example applications in Section 4. Furthermore, we describe our experiment setup in Section 5, and discuss the experiment results in Section 6. In addition, we discuss the possible extensions of this work in Section 7 and the prior work that is related to our system in Section 8. Finally, we conclude our work in Section 9.

## 2. Background

Different human-induced excitations induce different types of vibration signals. These signals mainly fall into two categories: the impulse and the slip-pulse signals [7,12]. In this section, we introduce the physics behind them, including 1) properties of waves induced by different types of excitations and 2) wave propagation in solids. Our signal characterization algorithm is designed based on the wave properties introduced here.

### 2.1. Impulse v.s. slip-pulse waves

The impulse and slip-pulse excitation on structures produce different mechanical waves. The former induces surface waves due to point impact force while the latter produces body waves due to friction.

Impact-induced vibrations are produced by a single point of contact on structures [7], such as a foot striking on a floor or a pen tapping on a table. The force applied to a structure causes it to deform. As the contact point is relieved of the force, the structure retracts due to its elasticity. This elasticity generates surface waves propagating outward from the point of contact, similar to ripples generated by dropping a stone into water [7].

Friction-induced vibrations are observed when two objects slide against each other. Stick-slip is a general form of friction that induces vibrations [17,18], such as a chair dragging on a floor or a pen swiping on a table. When an object slides on a structure, it will ‘stick’ because of static friction and the unevenness of the structural material, then the force applied to it causes it to overcome the static friction and slide or ‘slip’ [17,19]. When these two states are alternating, the friction between the object and the structure changes between static friction and kinetic friction [19]. Since typically static friction is larger than kinetic friction, such alternating friction causes a sudden jump in the velocity of the movement, resulting in slip pulse [17,19] along the swipe. These slip pulses induce a wave that travels at an angle in the material as a combination of different types of waves dominated by body wave [19]. In this work, we leverage this body wave to locate the slip pulses and estimate the trajectory of the consecutive slip pulses.

### 2.2. Wave propagation in solids

When waves propagate in solid, they disperse and attenuate. Different waves have different *dispersion effects*. For surface waves, different frequency components travel at different speeds in the range of 50–300 $ms^{-1}$ [11,20,21]. Therefore, when the wave travels through the solid, the dispersion introduces distortion into the vibration signal, making vibration-based localization a challenge [20].

Different waves have different *attenuation effects*. An impact-induced vibration (impulse) is dominated by surface waves (Rayleigh waves, spreading $\propto r^{-1/2}$) [21,22]. On the other hand, a friction-induced vibration (slip-pulse) is dominated by body waves (shear wave, spreading $\propto r^{-1}$) [22,23]. Using these wave propagation characteristics, we infer that the friction-induced vibrations decay faster than impulse-induced vibrations and thus have less reflection on edges. We utilize this difference in our algorithm design, which will be discussed in Section 3.

## 3. Excitation characterization system

In this section, we present our sensing system that characterizes the human activity excitations on structures, such as footsteps on the floor and interaction on flat solid surfaces. The system mainly consists three parts as shown in Fig. 1: structural vibration signal sensing, excitation signal acquisition, excitation tracking. First of all, we obtain the overall structural vibration signal through our sensing system (Section 3.1). Then the system acquires the excitation signal by 1) detecting and extracting the excitation signals through anomaly detection and 2) identifying through excitation identification module before tracked through a specific algorithm (Section 3.2). We then introduce the excitation tracking algorithm that targets at two different types of excitations (Section 3.3).

### 3.1. Sensing system

The sensing module obtains structural vibration with sensors placed on the target structure. The vibration sensors detect vibrations caused by the structural particles moving perpendicular to the contacting structure. These can be a variety of sensors, including piezoelectric accelerometer [24], capacitive distance [25], laser [26], etc. In our system, we use the Geophones (SM-24) [27] as the vibration sensors in our sensing system, because they are low-cost vibration sensors that are sensitive to waves investigated here.

The system requires a minimum of 3 sensors to enable tracking, and we applied 4 sensors for each sensing area in our system in this paper to add redundancy for system robustness. The signals are then amplified before digitization using an oscilloscope. We deploy the system on the surface of different structures, and it detects various excitation induced structural vibrations. The retail price in U.S. is around $60 [27], and similar products are available at a price of less than 1 dollar in China [28]. The prototype of the system with four sensors costs $250 with only sensors and op-amps. We estimate the commercial scale production can lower this price to $10 per sensing node (1 processing unit, 1 op-amp, and 1 sensor each node). When deployed in the building for human monitoring purpose, we estimate the deployment price is approximately $0.25 per sqft.

### 3.2. Excitation signal acquisition

The excitation signal acquisition takes two steps: first, the system detects the signal segments that are induced by the excitation and groups them into each individual event (Section 3.2.1); then, the system identifies the type of excitation for each event (Section 3.2.2).

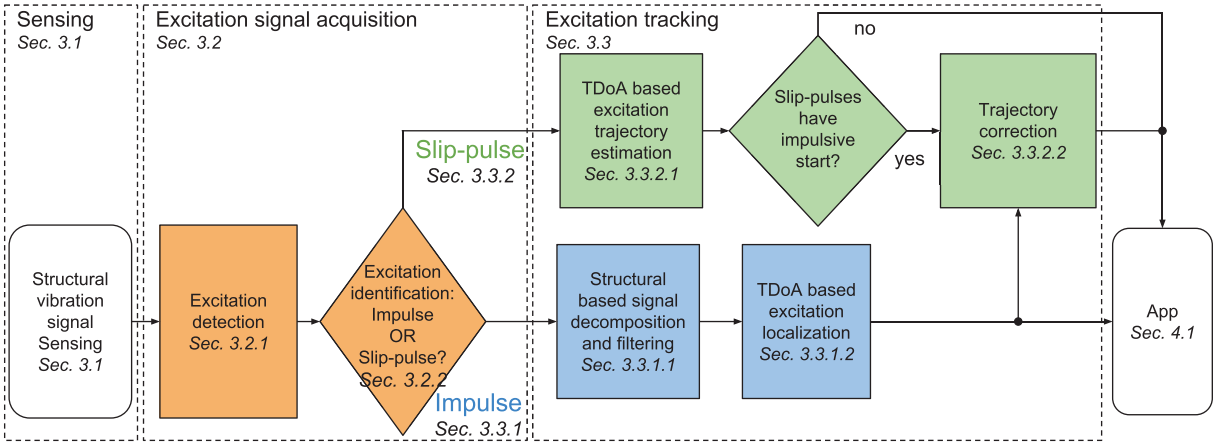


**Fig. 1.** Excitation characterization system overview.

*3.2.1. Excitation detection*

Intuitively, the excitation induced structural vibration has a higher signal energy than the noise signals. The excitation detection is conducted on the segmented signal windows, and the consecutive windows that are considered as excitation make an excitation event. The raw vibration signal is segmented into small windows to conduct excitation detection. For each windowed signal, we first calculate the signal energy. Then we determine whether each windowed signal is an excitation induced signal segment using anomaly detection [29]. To do so, a Gaussian noise model (mean $\mu$ and standard deviation $\sigma$) is calculated by the signal segments of ambient noise signals. Then, when an investigated segment's signal energy is beyond the value of $\mu+3\sigma$, the segment is detected as an interaction segment. The consecutive windows that are detected as anomalies make an excitation event.

*3.2.2. Excitation identification*

The wave properties of different types of excitations vary, and the algorithm takes the excitation type into account and proceeds with different processes based on that. Therefore, the system first needs to identify if an excitation is an impulse or a slip-pulse.

Intuitively, the impulse excitations decay fast within a short duration due to the dissipation of the energy, while the slip-pulse excitations often last over seconds with continuous high signal energy due to the overlapping of multiple stick-slip iterations during the movement as discussed in Section 2. Fig. 2 shows examples of different type of excitation: impulse and slip-pulse. Fig. 2(a) demonstrates vibration signals induced by footstep (impulse excitation sources) on the floor. Fig. 2(b) demonstrates vibrations induced by a pen swiping (slip-pulse excitation sources) on a wood plane.

The system identifies an event to be a slip-pulse if the segments above the threshold last over an empirical threshold of one second, which applies to most of the impulse signals on various testing surfaces, otherwise an impulse. This identification of excitation signal types enables the selection of signal processing methods to achieve highly accurate signal source tracking.

### 3.3. Excitation tracking

Once the system obtains the excitation signal and its type, it tracks the excitation accordingly. We first introduce the algorithm for impulse excitation localization (Section 3.3.1), then present the algorithm for slip-pulse excitation tracking (Section 3.3.2).

*3.3.1. Impulse excitation characterization: localization*

When an impulsive excitation occurs on a structure, the contact happens at a single point, therefore the information we focus on extracting for this type of signal is the excitation location. To localize the excitation point, the system first decomposes the vibration signal and filters based on the observed structural character (Section 3.3.1.1), then extracts TDoA from signals of different sensors and calculates the location of each excitation point (Section 3.3.1.2).

*3.3.1.1. Structure-based signal decomposition and filtering.* For impulse signals, wavelet-based decomposition is effective for band selection and filtering because the mother wavelet has high similarity with the shape of the fast-decaying oscillating waveform [20]. Fig. 3(a) demonstrates an example of impulse excitation signals obtained by two different sensors. The

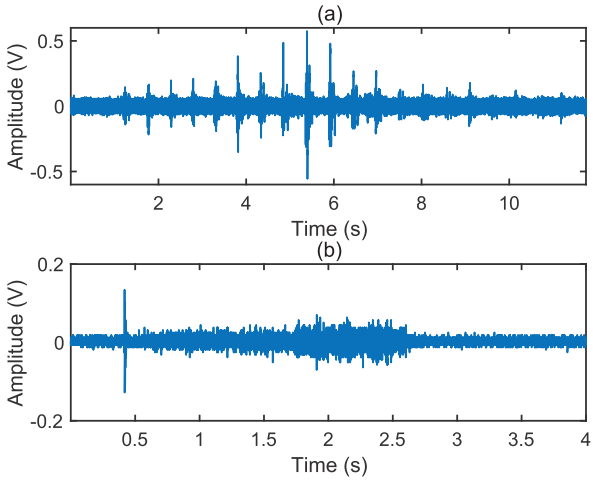


**Fig. 2.** Examples of human activity impacts that induce structural vibrations. (a) Footstep induced floor vibration signals. (b) Interaction swipe induced wood surface vibration signals. We demonstrate a sequence of footstep induced floor vibration signals when a person passes by the sensing area in (a) and the vibration signal of a wood plane when a pen swipes through the sensing area in (b). Different types of excitations induce different types of vibration signals.

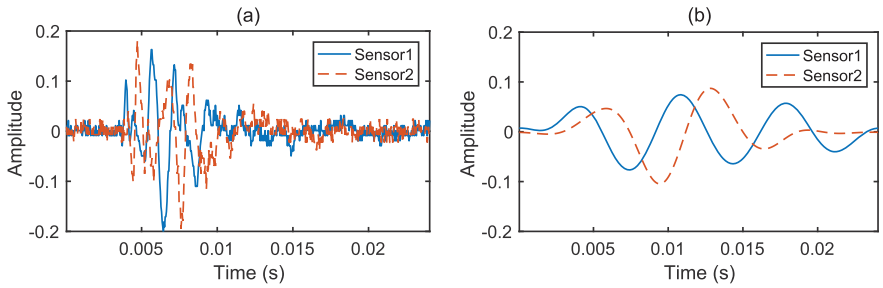


**Fig. 3.** Examples of impulse-like excitation signals obtained by different sensors before and after wavelet filtering. (a) Raw signals detected by two sensors. (b) Filtered signals detected by two sensors. The filtered signals in (b) show higher similarity compared to those in (a). It indicates that the filtering helps remove the dispersion effects.

original raw signal shows clear dispersion, causing the signal characteristics different from each other including the first peak and valley of the signal. The cross-correlation peak values for the original signal and the filtered signal are 0.62 and 0.84 respectively, shown a clear increase after the filtering is applied.

Then we decompose the signal with wavelet transform and reconstruct the signal on a specific scale, which is obtained through a simple calibration phase. We conduct this signal decomposition and show the filtered signal in Fig. 3(b). Compared to the raw signal in Fig. 3(a), the filtered signal demonstrates a higher similarity. Therefore, the wavelet filtering reduce the dispersion effects in the vibration signals significantly. It is an important step in our characterization system.

We present two ways to select the filtering scales: 1) We utilize the ambient noise signal and select the scale that has the highest signal energy. This gives us the fundamental frequency band for the floor structure, on which the signal travels farthest. 2) We conduct a low-cost calibration by generating impulse signals at known location (e.g., between each pair of sensors) for each sample board, and select the scale and velocity that cause least error at these designated points. This gives us the optimal parameters for the targeting area despite the material of the surface.

In this paper, we use the former on the human tracking application and the later on the interaction tracking. The human tracking application usually requires a larger scale deployment than that of the interaction application. Therefore, labor free scale selection is a better fit. On the other hand, calibration on a small human interaction area is easy to conduct, and the improvement in accuracy is significant and important for interaction purposes. We will further describe the details in later sections for each application.

*3.3.1.2. TDoA based excitation localization.* For impulse excitation signals, we conduct TDoA based localization with the filtered signal from Section 3.3.1.1. Various TDoA estimation methods have been explored for different deployment details [20,30]. We selected the first peak of arrival since the first peak is less likely to be impacted by reflections [11].

Then multilateration with the pairwise TDoA values from different sensors is used to estimate the excitation location. Multilateration is a common technique used to determine the location of a source by comparing the TDoA of signals with different distance towards different sensors [31]. For a pair of sensors, the difference in distances between them results in a hyperbolic curve with an infinite number of locations that satisfy the measurements. When there are multiple hyperbolic curves from different pairs of sensors, the location of their intersection is considered as the source location [20]. The Levenberg Marquardt algorithm [32] is used to find the solution of this intersection as a least square curve-fitting problem.

*3.3.2. Slip-pulse excitation characterization: trajectory estimation*

When a slip-pulse signal occurs on the structure, there is a sequence of contact points forming a trajectory. which can be described by the direction and the length. To obtain this information, the system first conducts the trajectory estimation by tracking the segments of the slip-pulse signal (Section 3.3.2.1). Based on the wave properties comparison in Section 2.2, we know slip-pulse signals have a higher attenuation rate, hence the frequency components are more concentrated, which enables the tracking of the unfiltered signals. Then, if there is an initial contact impulse signal, the system further conduct trajectory correction with the estimated location of the initial impulse excitation (Section 3.3.2.2).

*3.3.2.1. TDoA based excitation localization.* The intuition to obtain trajectory of the slip-pulse signals is that each segment of the continuous slip-pulse signal can be considered as a separate excitation source, and the locations of the sequence of these segments make the trajectory of the slip-pulse signal.

Fig. 4(a) shows an example of slip-pulse signals detected by two synchronized sensors. Fig. 4(c, d, e) show three segments selected at the fore-end, middle, and tail-end part of the signal marked out in Fig. 4(a) with black lines. Compared to impulses, slip pulses show more concentrated frequency components, as shown in Fig. 4(b, f). This is caused by the higher attenuation rate of the body wave, so that when the wave arrives at the sensor, some frequencies have already died down, leaving fewer frequency components, hinting at lower dispersion. In addition, the reflection may also be lower than that of impulses due to the higher attenuation rate. With less dispersion and reflection, correlation is visible between segments from different sensors without the need for wavelet analysis as shown in Fig. 4(c, d, e).

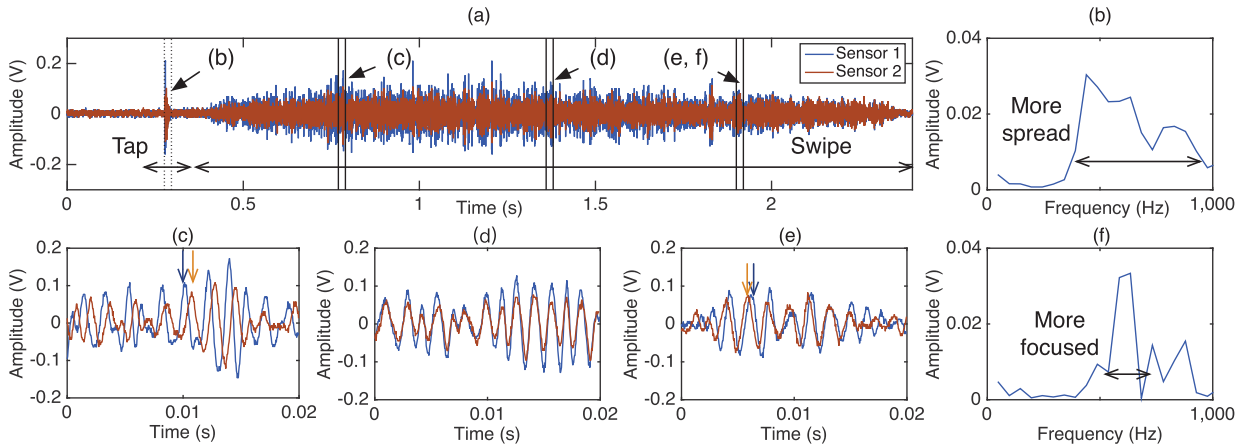


**Fig. 4.** Impulse and slip-pulse signal TDoA progression. (a) A slip-pulse excitation occurs from Sensor 1 to Sensor 2. (b) The frequency domain signal of the initial impulse. (c) The time domain signal of a fore-end segment. (d) The time domain signal of a middle segment. (e) The time domain signal of a tail-end segment. (f) The frequency domain signal of the tail-end segment in (e). Signals in (c) demonstrate a shift where the blue line is leading in time of arrival, meaning the signal source is closer to Sensor 1. (d) The red line and blue line have similar phase. (e) shows that in the end part of the signal, the shift is reversed as that shown in (c). (For interpretation of the references to colour in this figure legend, the reader is referred to the web version of this article.)

Unlike impulse excitations, there is no 'first peak' for a segment of a slip-pulse signal. Therefore, we extract TDoA using cross-correlation from multiple consecutive slip-pulses and localize each of them. Their locations make the trajectory of the slip-pulse excitation.

*3.3.2.2. Trajectory correction with initial contact induced impulse.* The slip-pulse excitations are generated by the friction between two objects. Therefore, for some applications, the system detects the initial impulse excitation from the contact of these two objects. As discussed in Section 3.3.2.1 and will be discussed in the evaluation in Section 6, the structure based signal decomposition applied on impulse signals allows the system to tolerate high signal dispersion effect. While dispersion is less of a concern with slip-pulse than with impulse signals, it can still impact the TDoA estimation. However, the wavelet filter is effective in removing dispersion effects with impulse excitation signals, which could be applied on the initial contact induced impulse signal right before the slip-pulse signal in time domain. Therefore, we utilize the initial contact induced impulse signal to further correct the trajectory estimated from the slip-pulse signal.

## 4. Example applications

Based on the excitation characterization system introduced in Section 3, we further introduce example applications to illustrate the system in realistic scenarios. We focus on building level and object level applications to demonstrate the robustness of our system.

### *4.1. Building level: human activity tracking*

Human indoor activity information enables various smart home applications, such as children/patient monitoring, appliance usage safety check, personalization services, etc. When people walk in an indoor environment, their activities (e.g., stepping, dragging objects, door closing, etc.) generate vibration signals that travel through floors. By extracting and tracking these everyday excitations, applications can further recognize the activities of the occupants in the building [33]. The excitations we target to trace in this scenario include footsteps falling and object dragging.

### *4.2. Object level: human interaction tracking*

Other than unintentional interaction with the physical environment, intentional interaction to create communication between human and devices is another important aspect in smart home applications. Intuitive and ubiquitous interaction methods enable better communication between human and devices. Therefore, another target application we investigate here is to provide ubiquitous human interaction methods by tracking the intentional interactions (such as tap and swipe) on a flat solid surface (such as walls and tables). The estimated location of interactions on a surface can be used as a control input of smart-home IoT devices, which may not have a direct interface due to the low power design. The excitations we target as the interaction include taps and swipes on multiple surfaces of different materials and sizes.

## 5. Example applications

In this section, we introduce the experimental design for the two applications discussed in Section 4. First, we describe the experiment procedure for each application implementation. Next, we explain the general sensing system setting of the experiment. Then we discuss the experiment parameters and experiment settings to accommodate these parameters.

### 5.1. Application I: human activity tracking

The experiment is conducted in a room with enough space to place sensors and step on the designated locations. The excitations investigated here include footsteps falling (impulse) and object dragging (slip-pulse). For foot strikes, the experiment is conducted in a room with wood floor. The sensor deployment is presented in Fig. 5(a).

Four sensors are deployed along a 4 m × 3 m sensing area to cover the sensing area and are illustrated as circles in the figure. They are placed to cover as large sensing area as possible. The crosses in Fig. 5(a) indicate the footstep locations. The number of footstep excitations collected at each location is 10.

For object dragging excitations, we conducted the experiment by dragging metal bars of different sizes and weights on a 60 cm × 60 cm wood platform. We selected the wood platform to avoid potential scratch damage to the floor surface. We selected metal bar to represent different types of objects that may be dragged through the floor, such as table and chair, and different size of metal bars allow us to control the weight of the slip-pulse signal with the rest of the parameter consistent. The metal bars are dragged through the platform surface as shown in Fig. 5(b).

### 5.2. Application II: human interaction tracking

The experiment is conducted in a room with enough space to place the largest surface investigated on the floor. For each scenario, the evaluated surface is placed at the same location in the room for consistency. Since the sample board is not coupled with the floor like these materials will appear in people's everyday life (e.g., as part of a table/wall), we represented real-world table/wall conditions by placing sand-filled weights (20 cm × 5 cm × 2 cm) around the sensing area in some experiments to enhance the coupling and damp the wave reflection at the loose edges. We use a pen to tap and swipe for consistency.

Compared to the human activity tracking experiment, the investigated sensing area in this case is in general smaller (<1 m × 1 m area) and the force applied on the structure is lower, despite the higher signal energy due to the short distance between sensor and excitations. On the other hand, due to the application difference, the accuracy of human interaction tracking application is higher than that of the human activity tracking.

### 5.3. General system settings

For both experiments, the data is collected at a sampling rate of 25 kHz to provide 1 cm resolution for up to 250 $ms^{-1}$ waves (Section 2.2) when used to estimate TDoA. To generate a slip-pulse signal with a controlled speed, we control the object moving speed with a metronome at a speed of 10 $cms^{-1}$. The segment window size is 0.02 s to cover a 0.2 cm distance, which is small enough to realize the resolution limitation of the system. The number of incidences for each scenario investigated is 10.

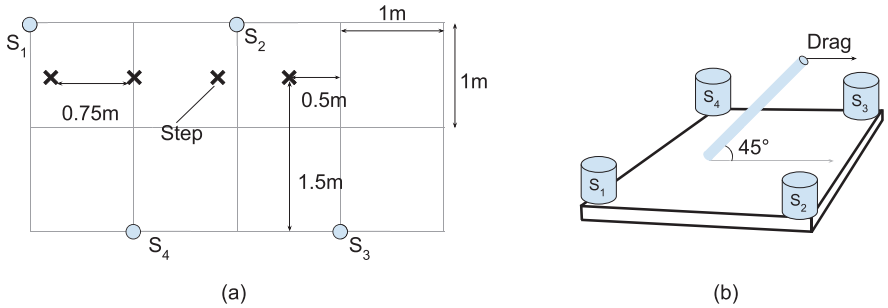


**Fig. 5.** Human activity induced excitation experiment setups. (a) Impulse (footstep) localization experiment settings. (b) Slip-pulse (object dragging) tracking experiment settings. We demonstrate the impulse localization experimental settings in (a): the blue circles represent sensor locations on a wood floor, and the black crosses represent footstep locations. We show the slip-pulse tracking experimental settings in (b): the blue cylinders are sensors, and the blue pipe is the metal bar dragged on the sample wood plate. (For interpretation of the references to colour in this figure legend, the reader is referred to the web version of this article.)

**Table 1**
Experiments summary.

| App | Structure | Type | Sec. | Excitation | Variable |
|---|---|---|---|---|---|
| I | floor | impulse | 6.2.1 | footstep | impulse location |
| II | sample | impulse | 6.2.2 | tap | structure material |
| II | sample | impulse | 6.2.2 | tap | structure size |
| II | sample | impulse | 6.2.2 | tap | distance between sensors |
| II | sample | impulse | 6.2.2 | tap | sensing area |
| I | sample | slip-pulse | 6.3.1 | drag | object weight (strength) |
| II | sample | slip-pulse | 6.3.2.1 | swipe | window size<br>pointer type |
| II | sample | slip-pulse | 6.3.2.2 | swipe | swipe length<br>swipe speed<br>swipe direction |
| II | sample | slip-pulse | 6.3.2.3 | swipe | structure material<br>structure size<br>distance between sensors<br>sensing area |

### 5.4. Experiment parameters

Various of parameters may affect the system performance, which mainly fall into three categories: 1) the implementation factors, 2) the excitation factors, and 3) the structural factors. These factors include structural material, structure size, sensing area size (distance between sensor pairs), excitation location on the sensing area, excitation strength, excitation type, etc. We summarize the experiment information in Table 1.

### 5.5. Sample board settings

Compared to Application I, Application II targets small scaled flat solid surfaces, which can be explored through various sampling boards. This allows us to understand system robustness through evaluations on different materials, surface sizes, sensor deployment distances, and different areas on the board as discussed in Section 5.4.

Five different surface materials are investigated, including wood, iron, cement, stone, and ceramic. These surfaces were chosen as a representation of materials and surfaces found in a person's everyday life, such as tables, cabinets, and walls. For the first four materials, we find samples of size 61 cm × 61 cm, therefore we set $B = 61$ cm, $S = 40$ cm shown in Fig. 6(a) as the baseline. The ceramic surface sample used here is 41 cm × 41 cm as it is the only size available.

To evaluate the margin size, we first set the specific sensor deployment setting (the board margin size $m$) $m = 1$ cm as shown in Fig. 6(a). Next, we vary $m$, from 1 cm to 30 cm, with intermediate values of 10 cm and 20 cm. The experiment is done on wood surfaces only, since wood can be cut into these sizes.

For the largest surface ($B = 101$ cm) we evaluate the sensing range by changing the value $S$ from 40 cm to 80 cm with incremental 10 cm. For each case, the tap and swipes are at the same location as shown in Fig. 6(b and c) within the central 40 cm × 40 cm area of the board. Furthermore, to evaluate effects on different parts of sensing area, we tap and swipe at locations shown in Fig. 6(d) on a surface of $B = 101$ cm, $S = 80$ cm.

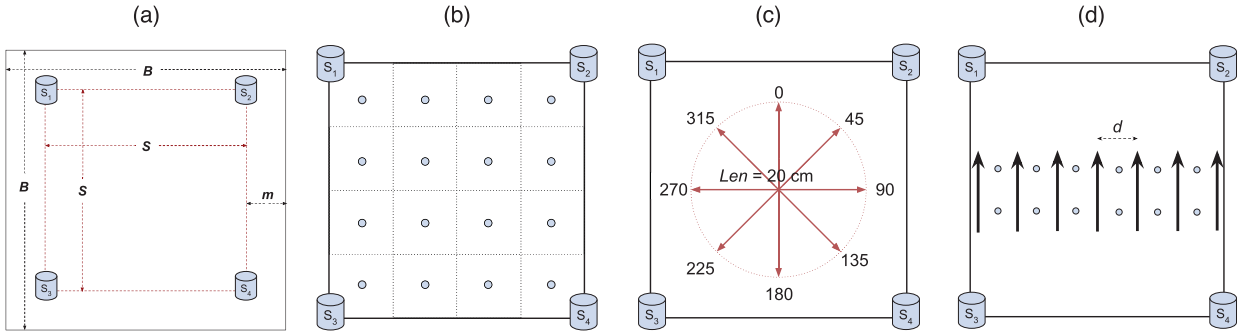


**Fig. 6.** Human interaction tracking experiment setup. (a) Surface settings. (b) Tap experiments. (c) Swipe experiments. (d) Effective area experiments. Dots and arrows indicate tap location and swipe length/direction respectively. (a) shows the surface setting, B is the size of the board, S is the size of the sensing area, defined as distance between sensors, m is the margin from sensing area to board edges. We evaluate different B and S combination with interactions shown in (b, c) within a 40 cm × 40 cm interaction area. (d) shows the effective area experiment setting with a 80 cm × 80 cm interaction area.

## 6. Example applications

To understand our algorithm performance, we conduct experiments on various structures based on the applications discussed in Section 4 and the experiment design described in Section 5. In this section, we first introduce the evaluation metrics in Section 6.1. Then we present and analyze the results of impulse localization in Section 6.2 and slip-pulse tracking in Section 6.3.

### 6.1. Metrics

We select the metrics as follows to evaluate the impulse localization and slip-pulse tracking estimation performance. For each metric, we evaluate both error and precision. The error and precision of impulse and slip-pulse excitations are different, therefore we define them separately in this section.

**Impulse Error.** For impulses, we measure the distance between the estimated location and the ground truth location as the localization error. The precision is measured by the scattering radius of the estimated location with the same ground truth location.

**Slip-pulse Error.** For slip-pulses, we measure the length and angle error of the estimated trajectory compared to the ground truth trajectory since we investigate linear trajectory in this paper. The length error is positive when the estimation length is longer than that of ground truth, and negative when shorter. The clockwise angle errors are considered as positive values, and the counter clock wise errors as negative values. Because of this, the standard deviation (referred as std for short in later sections) of the error would be effective to describe the system performance here since the average could be canceling out. The precision indicates the accuracy of the tracking in following the trajectory. It is measured by the distance between estimated location of each segment and the trajectory. In the following sections, we refer to it as trajectory error.

### 6.2. Evaluation I: impulse excitation localization

The challenge faced by impulse excitation localization through surface vibrations lies in the dispersion of wave propagation. We address that by studying properties of the impulse-induced surface wave and utilizing a wavelet filter to extract the designated scale of signals and reduce the dispersion effects. To evaluate our localization algorithm, we compare localization error rates when different methods are applied.

The footstep localization experiments evaluate the system performance in a specific structural condition (the floor in a room) and of a larger area. The tap localization experiments evaluate the 'micro' area (a sample surface) where we can further evaluate on different materials and surface sizes. The goal is to evaluate the performance of our system in handling the dispersion and attenuation effects. Therefore, in the example sections (Section 6.2.1, 6.2.2), we compare the localization accuracies with v.s. without applying the wavelet filter.

#### 6.2.1. Impulse example I: footstep

To understand the performance of the system with or without taking wave properties into account, we compare the footstep localization results in these two scenarios. Fig. 7(a) shows the accuracy of the estimated location of the four step demonstrated in Fig. 5 with boxplots.[1] The light box plot shows the system error rate without applying wavelet filter and the dark box plot shows the system error rate when the wavelet filter is applied. As mentioned in Section 3.3.1.1, the filter scale is selected based on the ambient noise vibration. The system conducts wavelet decomposition on the ambient noise signal and selects the scale with highest signal energy. The selected scale corresponds to the building fundamental frequency, on which the vibration signal travels the farthest [14]. The average location estimation error when the filter is not applied is 2.18 m, with the standard deviation of 1.88 m and median of 0.91 m, when the filter is not applied. This value drops to 0.49 m, with the standard deviation of 0.17 m and median of 0.46 m, when the structure-based decomposition is conducted and the signal is filtered based on that. The location estimation precision is shown in Fig. 7(b). The average precision values are 0.17 m and 0.07 m, with the median values of 0.13 m and 0.07 m respectively for the cases without and with the wavelet filter. In summary, the average localization error rate decreased four times, and the average location precision decreased twice.

#### 6.2.2. Impulse example II: Surface tap

To understand the system performance through different settings, we conducted experiments discussed in Section 5 and show the results here. As an example, Fig. 8 shows the tap localization results when the dispersion is handled through different methods. Fig. 8(a) shows the localization of raw signal and using cross-correlation to obtain TDoA estimation (the same as applied to the swipe segments). The four locations near the center show higher accuracy and precision than the rest. This is because the noise and dispersion make the TDoA estimation unstable when the tap point is far away from the board center. As discussed in Section 3.3.1.1, the calibration by generating impulse signal at designated locations to select the filtering scale is suitable for small scale deployment such as interaction tracking. We conducted the calibration and compared

[1] A box plot shows the mean (circle), median (middle line), quartiles (rectangle box), fences (outside box line), and outliers (cross markers) of the data points.

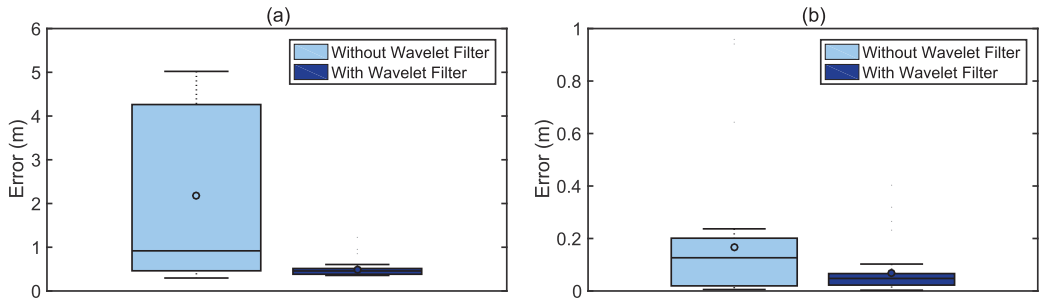


**Fig. 7.** Footstep localization results. (a) Localization error. (b) Localization precision. We observe that when the wavelet filter is applied, both the localization error and precision values decrease.

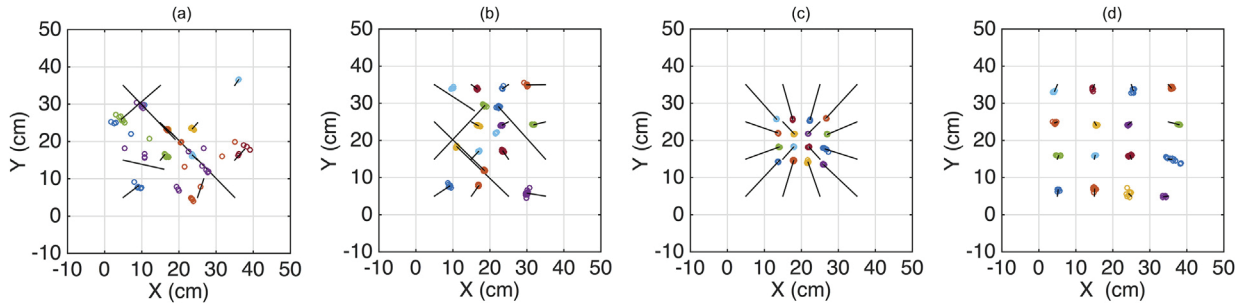


**Fig. 8.** Tap localization examples. Each tap location has 10 data points plotted in one color, they form a cluster and a line is drawn from the center of the cluster to the ground truth location. (a) No filter, no calibration. (b) Filter on a global band, no calibration. (c) Filter on a calibrated band, with lower bound velocity used. (d) Filter on a calibrated band, with calibrated velocity. The x-axis and y-axis are the dimensions of the sensing area. (For interpretation of the references to colour in this figure legend, the reader is referred to the web version of this article.)

the results in Fig. 8. Fig. 8(b) shows the results when the system filters the signal on a global band instead of a calibrated band. The results already shows higher accuracy compared to Fig. 8(a) and demonstrates high precision. Furthermore, when we calibrate the filtering band and only use the lower bound of the velocity for various materials, the results shows a high accuracy of the relative locations and a consistent offset to their absolute locations in Fig. 8(c). Finally, we show the results of both filtering band and wave velocity are selected from our calibration method with/without the surface edge damped in Fig. 8(d). The accuracy of the estimated location shows less than 3 cm error and high precision.

**Surface Tap: Surface Material.** Fig. 9 shows box plots of tap localization results on different materials. To understand the importance of band selection for different materials, we selected the global band as discussed in the last section to apply on all the materials, and the results are shown in Fig. 9. The estimations utilizing calibration on both wavelet filter band and calibrated velocity have consistently lower errors than without wavelet filter, with an average localization error reduction of

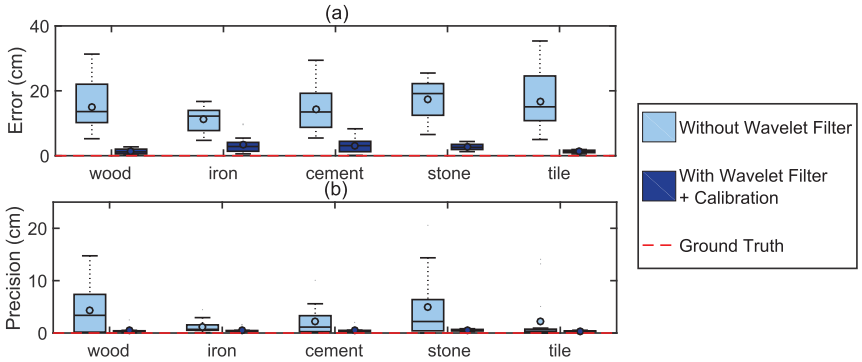


**Fig. 9.** Tap localization results on different materials. (a) Localization error. (b) Localization precision. The x-axis is the material type, and the y-axis is the error value. The light blue bars show the localization results when there is no filter applied, and the dark blue bars show that when there is a calibrated filter applied. When no filter is applied, the error rate is high for all materials. When the wavelet filtered is applied and the velocity is calibrated, the system achieves a six times lower average error rate through all tested materials. (For interpretation of the references to colour in this figure legend, the reader is referred to the web version of this article.)

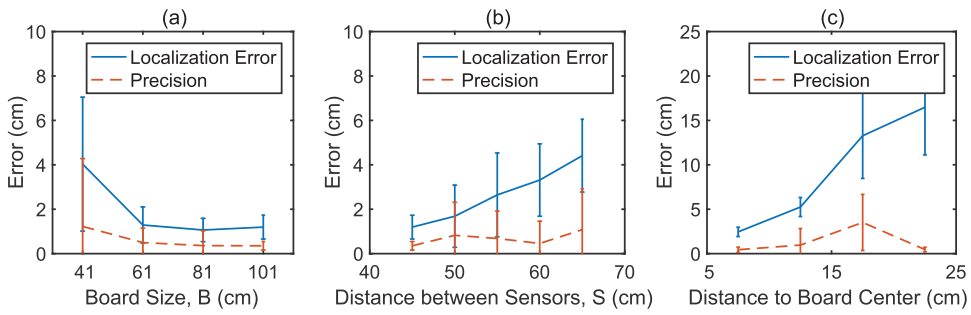


**Fig. 10.** Tap localization performance. (a) Localization error for board of different sizes. (b) Localization error for board settings with different between sensor distances. (c) Localization error for taps at different locations on a board. In general, settings with larger distance to edge and smaller sensing area achieve lower error rates due to less reflection and dispersion.

14.8 cm (six times). In addition, when filtered on the selected band, the precision error is lower than 0.5 cm, as compared to the 2.9 cm when no filter is applied. The results show that with the properly selected filtering band and wave velocity, the system achieves up to a six times lower localization error.

**Surface Tap: Margin Size.** For the same size of sensing area ($S = 40$ cm), different margin sizes including $m = 10$ cm, 20 cm, 30 cm} shows similar level of localization error (respectively 1.3 cm, 1.1 cm, and 1.2 cm) as shown in Fig. 10(a). For size $m = 1$ cm, the localization error is up to 4 cm. The size of the sensing area in this case is almost the same size as the board. As a result, the sensors are placed right at the corners of the board, where the boundary conditions could be more complicated. Furthermore, the smaller board resides less stably as taps are applied, resulting higher noise and error.

**Surface Tap: Distance between Sensors.** For the same size of interaction area and same size of surface, the difference in distance to sensing area also affects the sensing ability of the system. We investigate this factor by the surface setting of $B = 101$ cm, $S = 40$ cm, 50 cm, 60 cm, 70 cm, 80 cm. Fig. 10(b) shows the errors of localization and precision respectively. When the distance between the sensors and the sensing area increases, the average localization errors goes up from 1.2 cm to 4.4 cm. This is because of the fact that as the interaction area increases the calibrated velocity (average velocity for the entire board) is no longer well suited due to heterogeneity of the plywood material. That is also why the localization error increases while the precision error stays at a similar level.

**Surface Tap: Effective Sensing Area.** For the largest sensing area setting $B = 101$ cm, we further investigated the error rate for taps at different distance towards the center when the sensors are farthest from each other ($S = 80$ cm). Fig. 10(c) shows that the further the points are away from the center, the higher the localization errors are. When the distance of the tap is within 20 cm range from the center, the average localization error is 5.1 cm, while the taps outside this range have up to 18.4 cm average localization error. The precision error values are lower than 5 cm for all testing points. The increase of the localization error is caused by attenuation and dispersion, where the first peak decays to the noise level and cannot be detected.

### *6.3. Evaluation II: slip-pulse excitation tracking*

The slip-pulse excitations are tested through surfaces of different materials and settings. We evaluate different surfaces by comparing the parameters listed in Section 5.4. The system demonstrates robust interaction tracking through different parameter sets.

#### *6.3.1. Slip-pulse example I: metal bar dragging*

For the application of human activity tracking, we evaluate object dragging on the sample wood surface through metal bars of different weights. To control the weight consistently, we utilized metal bars with different weight and drag the bars through the designated trajectory without further pressing. Four metal bars with different weight (in a ratio of 1:1.5:2:2.5) are dragged through the testing trajectory, meaning the pressure is determined by the weight.

Fig. 11 shows the tracking results of the 4 bars dragging, and the results are averaged through eight investigating directions as shown in Fig. 6. The angle error standard deviation values are 36°, 31°, 42°, and 10° respectively. The length error average values are −4 cm, −3.3 cm, −4.5 cm, and −2.6 cm respectively. The results are shown a similar level of error for first 3 bars and the error rate is lower for the heaviest bar dragging.

#### *6.3.2. Slip-pulse example II: interactive swipe*

We investigate mainly three different types of information here: 1) system implementation parameters, including the sliding window size, the mounting condition, and the type of pointers used to perform scratch, 2) swipe parameters, including swipe direction and length, and 3) surface parameters, which is discussed in Section 5.4.

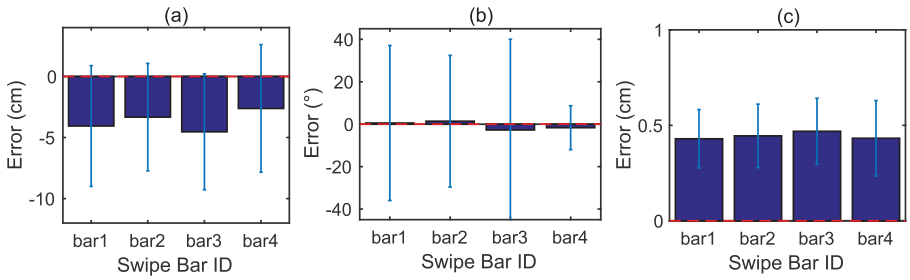


**Fig. 11.** Object dragging with objects of different weights tracking evaluation. (a) Length error. (b) Angle error. (c) Trajectory Error. The x-axis is the metal bar ID, and the y-axis is the error value. Four metal bars of different sizes/weights are used to drag through the test surface.

*6.3.2.1. Swipe: implementation factors.* There are three implementation factors that may affect the system performance: 1) test surface edge damping/mounting condition, 2) sliding window size used in the implementation, and 3) swipe instruments with the baseline algorithm. We conducted the experiments varying these factors on a wood surface of size $B = 61$ cm, since it is a size that allows modification of edge mounting condition.

**Window Size.** The sliding window size applied on the swipe signal determines the range of slip pulse covered in each window. Therefore, when the window size is too small, the signal might be too short to achieve an accurate match. On the other hand, when the window size is too large that it covers the signal segments with different TDoA values, the estimation of the TDoA of the entire windowed signal will be inaccurate. Therefore, we further evaluate the effect when different sliding window sizes are applied to swipe tracking. We experimented with five different window sizes, including 100, 200, 500, 1000, and 2000 samples per window. Since the sampling rate is 25 kHz, these windows are corresponding to the window size of 0.004, 0.008, 0.02, 0.04, and 0.08 s.

**Mounting Condition.** The swipe signal can be considered as a sequence of slip pulses, therefore if the reflection of preceding stick-slip signal does not die down after bouncing back at the edge, it will interfere with the later signal, and when a board is well mounted this is less likely. To prevent the reflection, we damp the edges of the investigated surfaces with sand-filled weights placed between edges and the sensing area, so that the wave energy dissipates to the weights before reaching to the edge.

Fig. 12 shows the length error, angle error, and trajectory error when varying the window size and the mounting condition. The x-axis shows the varying window size, and the y-axis shows the error rate of the corresponding metric. The light blue box plot shows the undamped experiment results, and the dark blue box plot shows the damped cases. When the window size is less than 500 samples, the angle error is relatively high because the order of the windows appearing may differently due to the mismatch of the TDoA estimation. For the undamped case, the average angle error values for 100-sample and 200-sample window are 68° and 52° respectively. Once the window size increased to over 500-sample, the error rate reduces to lower than 45° (26°, 1°, 3° respectively for 500-sample, 1000-sample, and 2000-sample). Similarly, the trajectory error is high when the window size is small, due to the TDoA estimation noise. We observe a clear decreasing trend (0.57 cm, 0.44 cm, 0.29 cm,

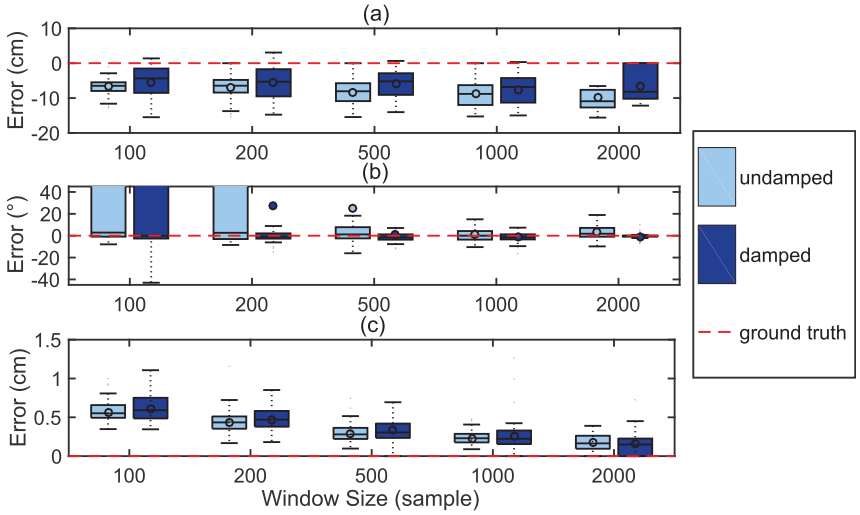


**Fig. 12.** Window size and mounting condition evaluation. (a) Length error. (b) Angle error. (c) Trajectory Error. The x-axis shows the varying window size, and the y-axis shows the error rate. When the window size is too small, the angle error is large. When the window size is too large, the length and trajectory error is large. The window size selection considers these metrics together. When the test surface is damped (mounted) the system shows lower errors in the experiments.

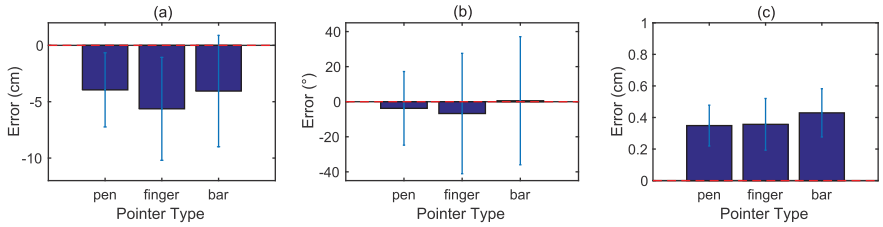


**Fig. 13.** Swipe pointer material evaluation. (a) Length error. (b) Angle error. (c) Trajectory Error. The x-axis is the pointer type, and the y-axis is the error value.

0.23 cm, and 0.18 cm) for the trajectory error when the window size increases. On the other hand, the length estimation error increases when the window size increase (−6.7 cm, −7 cm, −8.25 cm, −8.9 cm, and −9.8 cm). Therefore, by taking multiple evaluation metrics into account, we choose 500 sample (0.02 s) window size to proceed in the surface parameter evaluation later in Section 6.3.2.3, because it can achieve relatively accurate length estimation while maintaining a low angle and trajectory error rate. When the test surface is damped, the tracking results show a lower error rate for the window size of 500 in both length error and angle error.

**Pointer Material.** Three different materials including pen, fingernail, and metal bar are tested and the results are shown in Fig. 13. These three pointers are selected to represent three different levels of signal strength: the light swipe of the fingernail, the medium strength of the pen butt, and the heavy strength of the metal bar scratching. Each of the pointer is tested through 8 evaluating swipe directions, each containing 10 swipes.

We can observe from the figure that the pen and the bar achieve a similar level of length error value of −4 cm, while the weak scratch from fingernails shows slightly higher error value of −5.6 cm. These three pointers demonstrated a similar level of error on the other two metrics (angle and trajectory errors). This indicates that the system allows various pointers interaction in the real-world scenario, such as pen butt on a meeting table, fingernail on a wall, or a chopstick on a countertop. In the rest of the swipe evaluation, we used the pen to perform all the swipes due to its consistency.

*6.3.2.2. Swipe: swipe variables.* The parameters that describe a swipe include the length, the speed, and the direction. Therefore, in this section, we evaluate the system performance with different swipe direction and length. We investigate these experiments on a ceramic tile, which demonstrates high signal to noise ratio.

**Swipe Length.** For different sensing area, the system performance may vary due to different dispersion effect. Therefore, when the length of the swipe varies, the coverage of the swipes are different, therefore the dispersion effect for different length varies. Therefore, other than the 20 cm swipes we test on all scenarios, we further investigate a longer swipe of 30 cm to verify this assumption.

**Swipe Speed.** When the swipes occur at different speeds, a specific window size may cover slip pulses of different location range. Therefore, for the speed of the swipe varies, the optimal window size to characterize the excitation may vary. On the other hand, since the speeds of the excitation induced by human activities are limited, therefore, the potential error rate change is also within a limited range. To evaluate the speed difference caused performance change, we further evaluated the swipe with 8 $cms^{-1}$, a slower speed than the 10 $cms^{-1}$ that we tested in the rest of the evaluation section.

Fig. 14 shows the system performance of three combinations of the swipe lengths (*Len*) and swipe speeds (*Sp*): 1) $Len = 30$ cm, $Sp = 8$ $cms^{-1}$, 2) $Len = 20$ cm, $Sp = 8$ $cms^{-1}$, and 3) $Len = 30$ cm, $Sp = 10$ $cms^{-1}$. The light blue, medium blue, and dark blue box plots in (a, b, c) show these three combinations respectively, and (a, b, c) show the length error, angle error, and trajectory error of the investigated swipes respectively. In general, when the swipe length increases, the length error standard deviation increases, and the angle error decreases. This is because with more windowed signals, more reference points can be used to estimate the direction of the swipe.

**Swipe Direction.** The swipe signal can be considered as a sequence of slip pulses, therefore when swipe to different directions, the reflection combination on the edges may vary. We evaluate the interactive swipe tracking with linear swipes to

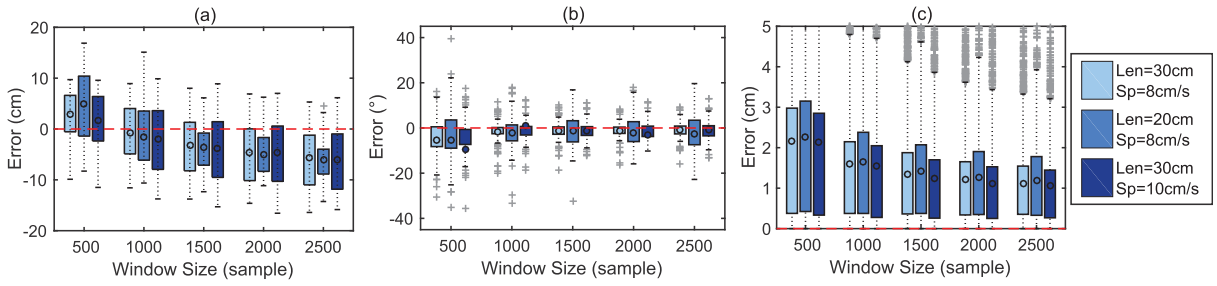


**Fig. 14.** Swipe length and speed v.s. window size. (a) Length error. (b) Angle error. (c) Trajectory Error. The x-axis shows the window size, the y-axis shows the error rate.

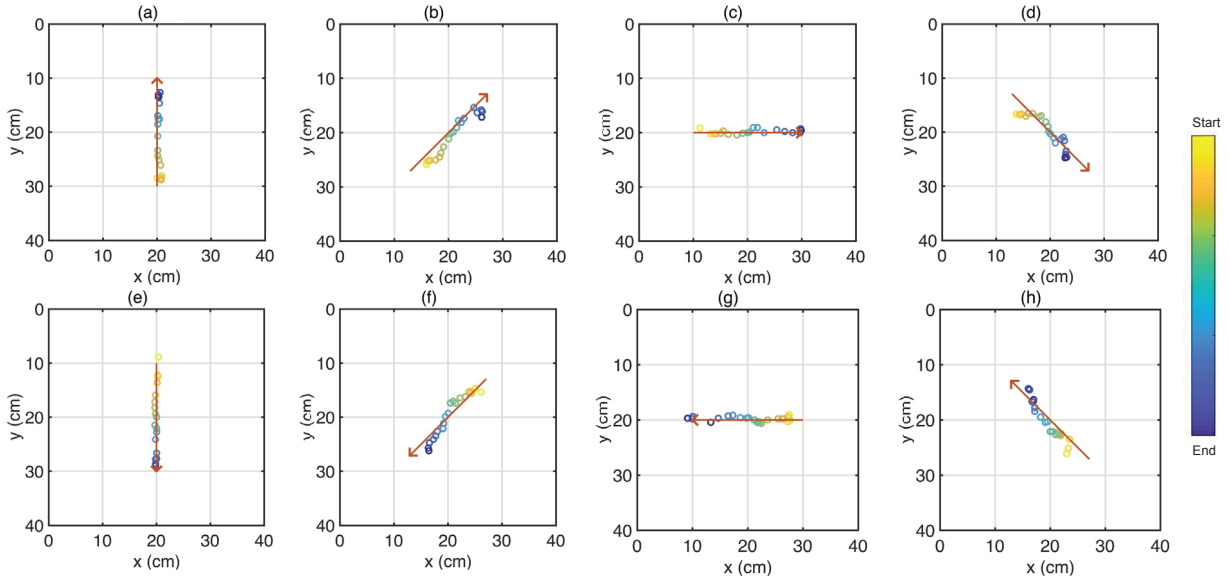


**Fig. 15.** Swipe examples. Swipes are decomposed into a series of localized points as detected by the algorithm. In (a–h), the expected directions and locations are noted by the red arrows. (For interpretation of the references to colour in this figure legend, the reader is referred to the web version of this article.)

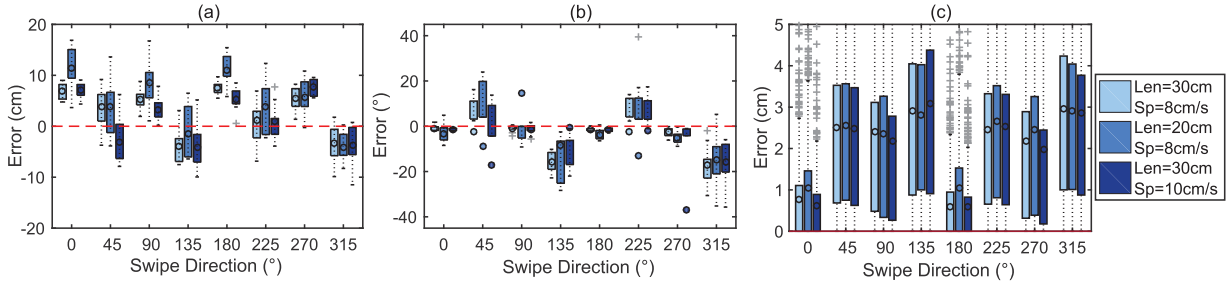


**Fig. 16.** Swipe length and speed v.s. swipe direction. (a) Length error. (b) Angle error. (c) Trajectory Error. The x-axis shows the swipe direction, the y-axis shows the error rate.

quantify the performance. Fig. 15(a–h) shows an example set of swipes detected by the system towards eight designated directions plotted in Fig. 6(c). We further plot the errors of investigated swipes by their directions of investigated swipes in Fig. 16. Different directions show different error rates, especially the trajectory errors shown in Fig. 16(c). This indicates the heterogeneity of the sample material, which causes different reflection effects.

*6.3.2.3. Swipe: surface parameters.* With the understanding of the system and swipe parameters, we controlled the parameters discussed above and further evaluate the effects of the surface parameters in this section.

**Swipe: Surface Material.** Different surface materials have different decay rates and reflection effects. Fig. 17 demonstrates the swipe accuracy for five investigated surface materials under four different processing scenarios: 1) undamped surface with baseline algorithm, 2) damped surface with baseline algorithm, 3) undamped surface with initial point correction, and 4) damped surface with initial point correction.

From the comparison in Fig. 17, we observe that for wood, iron, cement, and stone, the damped surface achieves lower error rate of length and angle. The average length estimation error over five materials is −8.7 cm for damped cases, and −10.3 cm for undamped cases. Similarly, the average angle error over five materials is −7.16° with std of 59.3° for damped cases, and −12.8° with std of 91.6° for undamped cases. The ceramic shows a different trend on length estimation when the damped surface is used. This could be caused by the different size of the ceramic sample due to the manufacturing limitation. Hence if we compare the first four materials, the damping reduced the average length error from −11.1 cm to −6.9 cm, and the average angle error from −15.5° with std of 96° to −2° with std of 39° (seven times reduction, twice reduction). We then further compare the scenarios where the initial tap localization is utilized v.s. those only rely on the estimation of the trajectory. The initial tap location scenarios achieved less length error in all cases, and on average the length error reduced from −10.5 cm to −8.1 cm. The average angle error reduced from −11.2 cm to −8.5 cm. While the trajectory error does not show a clear trend through different scenarios, it does have an average of less than 0.5 cm in all cases.

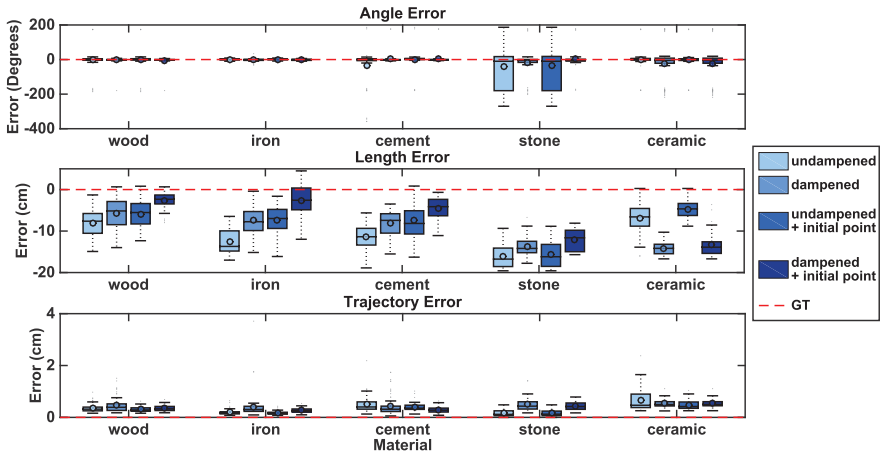


**Fig. 17.** Swipe material evaluation. (a) Length error. (b) Angle error. (c) Trajectory Error. The x-axis is material type, and the y-axis is error value. Five materials are evaluated through four processing methods. Our method shows highest error rate for first four materials, and both damping and using initial tap location allow system to achieve higher accuracy comparing to baseline. The ceramic shows opposite trends for damped and undamped comparison, which is caused by smaller size (only size available) and the damp is applied within the sensing area.

When the damp and initial tap trajectory correction were both applied, the average length error over five materials reduced from −11.3 cm to −7.2 cm (by a factor of 1.5), and the average angle error reduced from −14.6° with a standard deviation of 91° to −6.39° with a standard deviation of 61° (by a factor of 2). When comparing only the first four materials, this reduction is more clear from −12.2 cm to −4.6 cm (by a factor of 3) and 97°−37° (by a factor of 2.5) for average length error and standard deviation of angle errors, respectively. Therefore, both the damping and the trajectory correction contribute to reducing the length and angle errors. When both are applied, the system achieves the lowest error rate. This demonstrates the algorithm's robustness when tracking on surfaces of various materials.

**Swipe: Margin Size.** Fig. 18(a) demonstrates the results of four different sizes of wood boards with damped surfaces. When the board size is similar to the sensing area, the sensors are right at the corner of the board; hence experiencing the highest reflection effect. The average length error for the surface of $m = 1$ cm is −11 cm, while when $m$ increases to 10 cm, 20 cm, and 30 cm, the error is reduced to −5.4 cm, −8 cm, and −3.9 cm respectively. Similarly, the average angle error for the surface of $m = 1$ cm is 16° with a standard deviation of 101°, but when $m$ increases, the error standard deviation decreases to 30°, 46°, and 5°.We can observe a trend that when the margin between the board and the sensing area increases, the swipe error decreases, which we believe is due to the reduction of the reflection waves. When the surface size increases with the sensing area size remaining the same, it means that the distance between the board edge and the sensing area is increasing, which allows the reflection to die down before overlapping with the succeeding waves at the sensors.

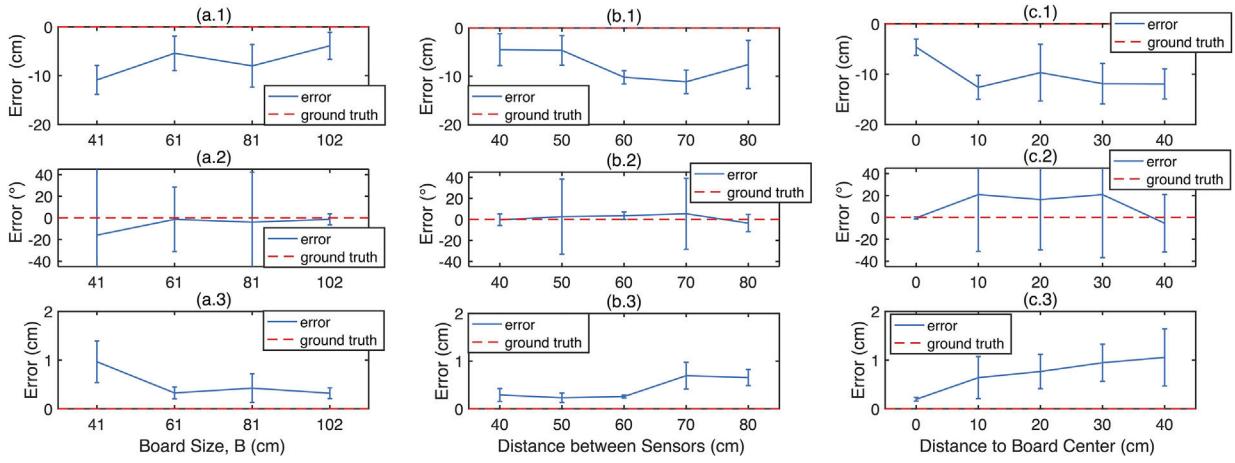


**Fig. 18.** Swipe surface setting evaluation. (a) Swipe margin size evaluation. When the surface size increases, i.e., margin between sensor and board edge increases, the error rate decreases, which is caused by the decrease of the reflection detected at the sensors. (a.1, a.2, a.3) are length error, angle error, and trajectory error respectively. (b) Swipe with different between-sensor distances. When between-sensor distances increase, the error rates increase. This is caused by dispersion effects, which are more severe when waves travel longer distance to sensors. (b.1, b.2, b.3) are length error, angle error, and trajectory error respectively. (c) Swipe to board center distance evaluation. The further the interaction from the board center the more severe the dispersion effect. (c.1, c.2, c.3) are length error, angle error, and trajectory error respectively. This is because the distances difference between sensors are increased, causing the waves to propagate longer distances.

**Swipe: Distance between Sensors.** The distance between sensors is the indication of the deployment density. The distance between sensors on large scaled surfaces will affect the attenuation rate of the interaction signal, as well as dispersion since the filtered signal is not a single band sine wave. Fig. 18(b) shows the five distances between sensors that we investigated. We observe that when the distance between sensors is increased, the average length error increases (respectively −5 cm, −4.7 cm, −10 cm, −11 cm}, and −7.6 cm). This trend is similar to the one that we observed in tap, which was caused by the emerging of the dispersion effect when the travel distance between the signal source and the sensor increases. The angle error std raises up to 35° when the distance between sensors are 50 cm and 70 cm. As we discussed with the tap evaluation, this change in angle error is due to the heterogeneity of the plywood surface.

**Swipe: Effective Sensing Area.** This experiment was conducted on the largest surface as described in Fig. 6(d). Swipes that are at different distances from the center were conducted and the swipe tracking results are shown in Fig. 18(c). The average angle error is 11° with a standard deviation of 42.6°. The length error and the trajectory error increased when the distance between the swipe and center was increased. The average length error for the center swipe (distance to board center is 0 cm) is −5 cm, while the rest are varying between −10 cm and −12 cm. Similarly, the angle error std increased tremendously from less than 1° to over 25° when the swipes are moved away from the center due to more severe dispersion as discussed in the tap evaluations.

## 7. Discussion

In this section, we explore the topics that further discuss the system robustness and possible extension from this paper based on the observations and conclusions we made from the evaluation section.

### 7.1. System robustness

To evaluate our excitation characterization system, we evaluated the system through different applications with various parameters through different excitation sources and structural settings. There are other aspects of the system robustness that we plan to further explore: 1) increasing excitation source types and 2) the heterogeneity of the structure/material.

Different excitation sources generate the vibration signal in different ways. For example, footstep or object dropping apply the force perpendicular to the floor and cause the deformation of the surface. Door/drawer closing applies the force to the wall/drawer surface and causes the surface to vibrate. When the surface vibration reaches the floor, it causes the floor to vibrate as well, hence can be localized. Since the excitation is relayed in this case, this wave propagation waits to be explored. The object dragging, as discussed in Section 6.3, causes friction horizontally to the surface, inducing slip-pulses, which alternates between static frictions and kinetic frictions. The wheel rolling, on the other hand, causes frictions that are dominated by static frictions. However, due to the slight unevenness of the wheel and floor surface, the bumpiness may induce a series of impulses vibrations that overlap with each other. Therefore, analyze more types of vibration sources can allow further human information learning such as activity recognition.

Most of the sample materials we investigated here are homogeneous, and we did observe the heterogeneity of the ceramic tiles in the discussion in Section 6.3.2.2. We also observe in heterogeneity of the floor with footstep signals. The structural elements in the floor such as beams and partitions demonstrates filtering effect when the wave propagates through them, which causes high frequency loss and high decay rate. Therefore, a more thorough characterization of these sources of heterogeneity may help the system to achieve higher tracking accuracy.

In summary, to achieve the robustness of the system, more characterization and processing are needed to recognize and handle the various scenarios we discussed here.

### 7.2. Multi-sources tracking

When there are multiple vibration sources in the sensing area, there are two major signal combinations that will happen: 1) the temporal combination sequence of different excitation sources, and 2) signal mixture by overlapping.

When there are multiple vibration sources in the environment that are triggered sequentially, such as footstep, door open/close, object dropping, etc., the system needs to analyze the continuity of different targeting sources to understand separated events. For example, if a person interacts with a table surface, while another person walks next to the table, the system can localize signal generated by these two different sources. Our prior work on human footstep detection classifies the signal segments induced by human footstep v.s. by other impulses [34]. Based on the signal characteristics and the detected location, the system can detect and identify the segments come from different sources.

Furthermore, when multiple vibration sources induced signals not only mix sequentially, but also overlap with each other, the localization problem faces two challenges: 1) the separation of the signal and 2) the localization of the separated signal. The traditional blind source separation methods can be applied to extract different signal characteristics. The filtering methods we discussed in this paper can help reduce the significant dispersion effects when the signal travels through different distances to reach the sensors and assist the separation algorithms. However the challenge remains, to obtain the location information, the pairwise shift for each separated impulses needs to be estimated. An alternative approach is to utilize the randomness of the human behavior, i.e., the overlapping human-induced impulse signals are not always synchronized completely. In addition, since the impulse signals has its rich frequency components concentrated at the onset of

**Table 2**
Performance summary of different sensing methods.

| Techniques | Vision | RF | Mobile | Acoustic | Load | Our Approach |
|---|---|---|---|---|---|---|
| Tracking Error (m) | ≤1 [37] | 0.25 [6] | ≤2 [50] | 0.17 [30] | tile size [2] | 0.21 [14] |
| Interaction Error (mm) | 10 [60] | NA | 37 [44] | NA | 0.002 [61] | 30 [16] |
| Identification Accuracy (%) | 95 [40] | 80 [46] | 85 [49] | 90 [53] | 93 [2] | 96 [62] |
| Detection Accuracy (%) | 98 [41] | 100 [47] | 87.4 [51] | 97 [54] | 100 [59] | 99.6 [29] |
| Deployment Density | Low | High | NA | Low | Very high | Low |
| Carrying Device | No | No | Yes | No | No | No |
| Privacy Conditions | Poor | Good | Poor | Poor | Good | Good |

the signal [35], the extraction of signal characteristics on partial signal can be also used for localizing multiple partially overlapping impulse signals.

### 7.3. Edge reflection & surface mounting

The wave reflection has a large impact on vibration based sensing methods as discussed in Section 6.3. In this paper, we utilized sand weights to reduce the wave reflection at edges, to simulate the following scenarios in real-world settings: 1) the surface is tightly mounted to a solid, such as kitchen counter top; and 2) the target surface area is surrounded by dissipating weights, such as books on a table. The tighter the surface is mounted, the higher the slip-pulse tracking accuracy will be (Section 6.3.2.3). As for extreme cases: 1) ground-coupled/wall-coupled surfaces that are tightly attached to a stable entity, and 2) loose surfaces like tables with thin legs, we expect the former to show higher accuracy and the later may show lower accuracy than the results demonstrated in the evaluation section. To make the system more robust to different reflection conditions (e.g., fixed end v.s. free end) [36], further physical insights and how to utilize them to reduce the reflection effects can be explored.

## 8. Related work

In this section, we mainly discuss prior works on human activity induced vibration in three aspects: 1) the sensing methods that have been proposed to achieve human activity learning, specifically on tracking of the activity and human interaction, 2) the human activity information learning from everyday excitation induced structural vibration, 3) physics driven methods to infer the vibration source information.

### 8.1. Indoor human information sensing systems

Many different sensing approaches have been proposed through the last decades [1], targeting to extract information about human in the indoor environment, including presence, count, location, identity, and activity. They can be categorized by sensing methods as follows: vision-, RF-, mobile-, acoustic-, and load-based methods. Vision-based methods tracks human and their interaction by recognizing their targeting tracking point (e.g., head, foot, hand, etc.) and localizing the point in the 3D perspective of the camera view [37–41]. The vision-based methods usually provides accurate information extraction (including tracking, interaction, and identification), if the light-of-sight between the target point and the camera is satisfied. In addition, vision-based methods often cause privacy concerns. RF-based methods [6,42–47] either require high density sensor deployment or yields low resolution on the tracking accuracy. Mobile devices [48–52] that are equipped with inertial sensors can provide tracking information as well with a specific device held by the user. Acoustic-based methods [30,53–57] either requires the user to be equipped with the special wearable devices, or are limited by the sensing conditions (limited resolution and range). Load-based methods [2,58,59] achieve high accuracy on the interaction point via high density sensor deployment. Compared to these prior methods, we focus on localizing vibration induced by the interaction on the surface of objects, which allows sparse sensing and high resolution tracking. We summarized the performance, as well as pros and cons of these methods in Table 2.[2]

### 8.2. Human information inferring through structural vibration sensing

Structural vibration sensing provides sparse and non-intrusive solution for obtaining human information. The foundation of this type of sensing method lies in the excitation induced by human activities that interact with the structures.

The information people extract mainly falls into the following categories: presence, count, identity, tracking, activity, status. When there is a human induced structural vibration detected, the presence of the people is detected. Work has been done on identify the floor vibrations that are induced by human footstep from other impulses to achieve the presence detection [34,63]. When multiple people interact with the physical surroundings, the vibration signal induced by different

[2] For the methods that does not provide enough resolution for direct interaction tracking, we put NA in the table.

people will be mixed. Therefore, when the mixed signal is detected by multiple sensors at different location, the features can be extracted across these sensors and then be used to estimate the number of people in the sensing environment [64,65]. Since human gait is a unique bio-metric that can be applied to identify individuals, the footstep induced vibration can be used to infer such information [62,66,67]. The tracking of the excitation sources enables indoor human tracking through different approaches that enable different tracking resolutions [29,68,69]. As for activity, such as interaction with the structure, has also been explored through different approaches, including machine learning approaches [9,10,70] and localization approaches [11–13,16]. Recently, work has been done on the health monitoring through structural vibration sensing that targets micro signals induced by human body such as heart rate [15].

The factors that distinguish our work from the prior work include 1) we generalized the excitation characterization (tracking to be more specific) system that can be applied on various structures and for different types of excitations. From the shown results, we can observe that the dispersion causes high deviation in localization results. In comparison, our work reduces the dispersion by addressing the nature of impulse and slip pulse waves, thus enabling vibration based approach on multiple less ideal materials. We are the first to utilize the wave properties to achieve accurate tracking of various excitation sources on multiple structures.

### 8.3. Human activity induced excitation tracking and characterization

In this paper, we demonstrated that utilizing physics information can assist our system in achieving robust human activity induced excitation (vibration source) tracking through different materials. Work has been done on robust vibration source tracking and characterization using physical principles, despite limited sensing data/labeling and human involvement [15,16,69,71,72]. Jia et al. utilize bed vibration to estimate human heart rate by analyzing the wave propagation model [15]. Han et al. measure vibrations of the vehicles to estimate their relative location (whether on the same lane) utilizing the physics insight of the vehicle vibration and road conditions [72]. Xu et al. use structural vibrations to infer traffic condition in the street [71]. Mirshekari et al. present the footstep localization in dispersive structures specifically and how to utilize physical information about the structure to assist sensing [69]. Pan et al. estimates the human-surface interaction locations by taking different excitation types (tap and swipe) into account in the tracking algorithm [16]. These prior works are all focused on a specific application, and in this paper we introduce our excitation characterization system, which is a general approach that can applied on many different applications.

## 9. Conclusion

In this paper, we presented a vibration-based sensing system that characterizes human activity induced impulse and slip-pulse excitations. We study properties of waves induced by different excitations and utilize these properties to reduce effects of dispersion and to enable accurate localization and tracking of impulses and slip-pulses. We further characterize different surface materials and settings to evaluate the accuracy and robustness of the system. For impulse excitations, our wavelet filter and calibration method achieves a six times improvement in localization error. For slip-pulse excitations, our algorithm achieves a three times improvement in length estimation error. Our system can enable ubiquitous human activity and interaction tracking for many future smart home applications.

## Ethics statement

This study was carried out in accordance with the recommendations of “CMU IRB Consent Form” with written informed consent from all subjects. All subjects gave written informed consent in accordance with the Declaration of Helsinki. The protocol was approved by the “CMU IRB committee,” IRB Protocol Number: HS15-009.

## Acknowledgements

This work is partially supported by NSF (CNS-1149611 and CMMI-1653550), Intel, Pennsylvania Infrastructure Technology Alliance (PITA), and Google.

## References

[1] T. Teixeira, G. Dublon, A. Savvides, A survey of human-sensing: methods for detecting presence, count, location, track, and identity, ACM Comput. Surv. 5 (1) (2010) 59–69.
[2] R.J. Orr, G.D. Abowd, The smart floor: a mechanism for natural user identification and tracking, in: CHI'00 Extended Abstracts on Human Factors in Computing Systems, ACM, 2000, pp. 275–276.
[3] P. Henry, M. Krainin, E. Herbst, X. Ren, D. Fox, Rgb-d mapping: using kinect-style depth cameras for dense 3d modeling of indoor environments, Int. J. Robot. Res. 31 (5) (2012) 647–663.
[4] Y. Zhang, C. Luo, J. Liu, Walk & sketch: create floor plans with an rgb-d camera, in: Proceedings of the 2012 ACM Conference on Ubiquitous Computing, ACM, 2012, pp. 461–470.
[5] C. Sertatıl, M.A. Altınkaya, K. Raoof, A novel acoustic indoor localization system employing cdma, Digit. Signal Process. 22 (3) (2012) 506–517.
[6] K. Qian, C. Wu, Z. Yang, Y. Liu, K. Jamieson, Widar: decimeter-level passive tracking via velocity monitoring with commodity wi-fi, in: Proceedings of the 18th ACM International Symposium on Mobile Ad Hoc Networking and Computing, ACM, 2017, p. 6.

[7] H. Bachmann, W. Ammann, Vibrations in Structures: Induced by Man and Machines, vol. 3, Iabse, Zurich, Switzerland, 1987.
[8] J. Poston, M. Buehrer, V. Malladi, A. Woolard, Vibration sensing in smart buildings for indoor positioning of pedestrians, in: Proceedings of the 2015 International Conference on Indoor Positioning and Indoor Navigation (IPIN), ACM, 2015, p. D2a.
[9] C. Harrison, S.E. Hudson, Scratch input: creating large, inexpensive, unpowered and mobile finger input surfaces, in: Proceedings of the 21st Annual ACM Symposium on User Interface Software and Technology, ACM, New York, NY, USA, 2008, pp. 205–208.
[10] C. Harrison, J. Schwarz, S.E. Hudson, Tapsense: enhancing finger interaction on touch surfaces, in: Proceedings of the 24th Annual ACM Symposium on User Interface Software and Technology, ACM, Santa Barbara, California, 2011, pp. 627–636.
[11] J.A. Paradiso, C. King Leo, Tracking and characterizing knocks atop large interactive displays, Sens. Rev. 25 (2) (2005) 134–143.
[12] D.T. Pham, Z. Ji, M. Yang, Z. Wang, M. Al-Kutubi, A novel human-computer interface based on passive acoustic localisation, in: International Conference on Human-computer Interaction, Springer, Beijing, China, 2007, pp. 901–909.
[13] R. Xiao, G. Lew, J. Marsanico, D. Hariharan, S. Hudson, C. Harrison, Toffee: enabling ad hoc, around device interaction with acoustic time-of-arrival correlation, in: Proceedings of the 16th International Conference on Human-computer Interaction with Mobile Devices & Services, ACM, 2014, pp. 67–76.
[14] M. Mirshekari, S. Pan, P. Zhang, H.Y. Noh, Characterizing wave propagation to improve indoor step-level person localization using floor vibration, in: SPIE Smart Structures and Materials+ Nondestructive Evaluation and Health Monitoring, International Society for Optics and Photonics, 2016, 980305–980305.
[15] Z. Jia, M. Alaziz, X. Chi, R.E. Howard, Y. Zhang, P. Zhang, W. Trappe, A. Sivasubramaniam, N. An, Hb-phone: a bed-mounted geophone-based heartbeat monitoring system, in: Information Processing in Sensor Networks (IPSN), 2016 15th ACM/IEEE International Conference, IEEE, Vienna, Austria, 2016, pp. 1–12.
[16] S. Pan, C. Ramirez, M. Mirshekari, J. Fagert, A.J. Chung, C.C. Hu, J.P. Shen, H.Y. Noh, P. Zhang, Surfacevibe: vibration-based tap & swipe tracking on ubiquitous surfaces, in: Information Processing in Sensor Networks (IPSN), 2017 15th ACM/IEEE International Conference, IEEE, 2017, pp. 1–12.
[17] G. Adams, Radiation of body waves induced by the sliding of an elastic half-space against a rigid surface, J. Appl. Mech. 67 (1) (2000) 1–5.
[18] R. Leine, D. Van Campen, A. De Kraker, L. Van Den Steen, Stick-slip vibrations induced by alternate friction models, Nonlinear Dyn. 16 (1) (1998) 41–54.
[19] B. Persson, Sliding Friction: Physical Principles and Applications, Springer Science & Business Media, Berlin, 2013.
[20] M. Mirshekari, S. Pan, P. Zhang, H.Y. Noh, Characterizing wave propagation to improve indoor step-level person localization using floor vibration, in: SPIE Smart Structures and Materials+ Nondestructive Evaluation and Health Monitoring, International Society for Optics and Photonics, Las Vegas, NV, USA, 2016, 980305–980305.
[21] I.A. Viktorov, Rayleigh and Lamb Waves: Physical Theory and Applications, Plenum Press, Berlin, Germany, 1970.
[22] H. Verhas, Prediction of the propagation of train-induced ground vibration, J. Sound Vib. 66 (3) (1979) 371–376.
[23] V.A. Yastrebov, Sliding without slipping under coulomb friction: opening waves and inversion of frictional force, Tribol. Lett. 62 (1) (2016) 1–8.
[24] F.A. Levinzon, Fundamental noise limit of piezoelectric accelerometer, IEEE Sens. J. 4 (1) (2004) 108–111.
[25] K.-L. Chau, S. Lewis, Y. Zhao, R. Howe, S. Bart, R. Marcheselli, An integrated force-balanced capacitive accelerometer for low-g applications, Sens. Actuators A Phys. 54 (1–3) (1996) 472–476.
[26] H.H. Nassif, M. Gindy, J. Davis, Comparison of laser doppler vibrometer with contact sensors for monitoring bridge deflection and vibration, Ndt E Int. 38 (3) (2005) 213–218.
[27] Geophone Sm-24, 2006. https://www.sparkfun.com/products/11744. (Accessed 24 January 2017).
[28] Geophone gd-28, 2013. https://world.taobao.com/item/18954260795.htm?fromSite=main&spm=a1z3o.7695460.0.0.31P2hg. (Accessed 24 January 2017).
[29] S. Pan, A. Bonde, J. Jing, L. Zhang, P. Zhang, H.Y. Noh, Boes: building occupancy estimation system using sparse ambient vibration monitoring, in: SPIE Smart Structures and Materials+ Nondestructive Evaluation and Health Monitoring, International Society for Optics and Photonics, San Diego, CA, USA, 2014, 90611O–90611O.
[30] Z. Sun, A. Purohit, K. Chen, S. Pan, T. Pering, P. Zhang, Pandaa: physical arrangement detection of networked devices through ambient-sound awareness, in: Proceedings of the 13th International Conference on Ubiquitous Computing, ACM, Beijing, China, 2011, pp. 425–434.
[31] A. Mandal, C.V. Lopes, T. Givargis, A. Haghighat, R. Jurdak, P. Baldi, Beep: 3d indoor positioning using audible sound, in: Consumer Communications and Networking Conference, 2005. CCNC. 2005 Second IEEE, IEEE, Las Vegas, NV, USA, 2005, pp. 348–353.
[32] D.W. Marquardt, An algorithm for least-squares estimation of nonlinear parameters, J. Soc. Ind. Appl. Math. 11 (2) (1963) 431–441.
[33] P. Kodeswaran, R. Kokku, M. Mallick, S. Sen, Demultiplexing activities of daily living in iot enabled smarthomes, in: Computer Communications, IEEE INFOCOM 2016-The 35th Annual IEEE International Conference, IEEE, 2016, pp. 1–9.
[34] M. Lam, M. Mirshekari, S. Pan, P. Zhang, H.Y. Noh, Robust occupant detection through step-induced floor vibration by incorporating structural characteristics, in: Dynamics of Coupled Structures, vol. 4, Springer, 2016, pp. 357–367.
[35] S. Pan, K. Lyons, M. Mirshekari, H.Y. Noh, P. Zhang, Multiple pedestrian tracking through ambient structural vibration sensing: poster abstract, in: Proceedings of the 14th ACM Conference on Embedded Network Sensor Systems CD-ROM, ACM, Stanford, California, 2016, pp. 366–367.
[36] R. Gregory, I. Gladwell, The reflection of a symmetric rayleigh-lamb wave at the fixed or free edge of a plate, J. Elast. 13 (2) (1983) 185–206.
[37] F. Fleuret, J. Berclaz, R. Lengagne, P. Fua, Multicamera people tracking with a probabilistic occupancy map, IEEE Trans. Pattern Anal. Mach. Intell. 30 (2) (2008) 267–282.
[38] Z. Ren, J. Yuan, J. Meng, Z. Zhang, Robust part-based hand gesture recognition using kinect sensor, IEEE Trans. Multimed. 15 (5) (2013) 1110–1120.
[39] G. Marin, F. Dominio, P. Zanuttigh, Hand gesture recognition with leap motion and kinect devices, in: Image Processing (ICIP), 2014 IEEE International Conference, IEEE, 2014, pp. 1565–1569.
[40] A. Kale, N. Cuntoor, B. Yegnanarayana, A. Rajagopalan, R. Chellappa, Gait Analysis for Human Identification, in: International Conference on Audio-and Video-based Biometric Person Authentication, Springer, 2003, pp. 706–714.
[41] C.A. Luna, C. Losada-Gutierrez, D. Fuentes-Jimenez, A. Fernandez-Rincon, M. Mazo, J. Macias Guarasa, Robust people detection using depth information from an overhead time-of-flight camera, Expert Syst. Appl. 71 (2017) 240–256.
[42] Q. Pu, S. Gupta, S. Gollakota, S. Patel, in: Whole-home Gesture Recognition Using Wireless Signals, in: Proceedings of the 19th Annual International Conference on Mobile Computing & Networking, ACM, 2013, pp. 27–38.
[43] F. Adib, Z. Kabelac, D. Katabi, R.C. Miller, 3d tracking via body radio reflections, in: NSDI, vol. 14, 2014, pp. 317–329.
[44] J. Wang, D. Vasisht, D. Katabi, Rf-idraw: virtual touch screen in the air using rf signals, in: ACM SIGCOMM Computer Communication Review, vol. 44, ACM, 2014, pp. 235–246.
[45] H. Abdelnasser, M. Youssef, K.A. Harras, Wigest: a ubiquitous wifi-based gesture recognition system, in: Computer Communications (INFOCOM), 2015 IEEE Conference, IEEE, 2015, pp. 1472–1480.
[46] Y. Zeng, P.H. Pathak, P. Mohapatra, Wiwho: wifi-based person identification in smart spaces, in: Proceedings of the 15th International Conference on Information Processing in Sensor Networks, IEEE Press, 2016, p. 4.
[47] M. Youssef, M. Mah, A. Agrawala, Challenges: device-free passive localization for wireless environments, in: Proceedings of the 13th Annual ACM International Conference on Mobile Computing and Networking, ACM, 2007, pp. 222–229.
[48] S. Cho, J.K. Oh, W. Bang, W. Chang, E. Choi, Y. Jing, J. Cho, D.Y. Kim, Magic wand: a hand-drawn gesture input device in 3-d space with inertial sensors, in: Frontiers in Handwriting Recognition, 2004. IWFHR-9 2004. Ninth International Workshop, IEEE, 2004, pp. 106–111.
[49] J. Mantyjarvi, M. Lindholm, E. Vildjiounaite, S. Makela, H. Ailisto, Identifying users of portable devices from gait pattern with accelerometers, in: Acoustics, Speech, and Signal Processing, 2005. Proceedings. (ICASSP'05). IEEE International Conference, vol. 2, IEEE, 2005, pp. ii–973.
[50] H. Liu, Y. Gan, J. Yang, S. Sidhom, Y. Wang, Y. Chen, F. Ye, Push the limit of wifi based localization for smartphones, in: Proceedings of the 18th Annual International Conference on Mobile Computing and Networking, ACM, 2012, pp. 305–316.

[51] W. Qin, J. Zhang, B. Li, L. Sun, Discovering human presence activities with smartphones using non-intrusive wi-fi sniffer sensors: the big data prospective, Int. J. Distrib. Sens. Netw. 9 (12) (2013) 927940.
[52] Y. Zheng, G. Shen, L. Li, C. Zhao, M. Li, F. Zhao, Travi-navi: Self-deployable Indoor Navigation System, IEEE/ACM Transactions on Networking.
[53] Z. Zhang, A.G. Andreou, Human identification experiments using acoustic micro-doppler signatures, in: Micro-nanoelectronics, Technology and Applications, 2008. EAMTA 2008, Argentine School of, IEEE, 2008, pp. 81–86.
[54] S.P. Tarzia, R.P. Dick, P.A. Dinda, G. Memik, Sonar-based measurement of user presence and attention, in: Proceedings of the 11th International Conference on Ubiquitous Computing, ACM, 2009, pp. 89–92.
[55] S. Gupta, D. Morris, S. Patel, D. Tan, Soundwave: using the doppler effect to sense gestures, in: Proceedings of the SIGCHI Conference on Human Factors in Computing Systems, ACM, 2012, pp. 1911–1914.
[56] H. Watanabe, T. Terada, M. Tsukamoto, Ultrasound-based movement sensing, gesture-, and context-recognition, in: Proceedings of the 2013 International Symposium on Wearable Computers, ACM, 2013, pp. 57–64.
[57] K.-Y. Chen, D. Ashbrook, M. Goel, S.-H. Lee, S. Patel, Airlink: sharing files between multiple devices using in-air gestures, in: Proceedings of the 2014 ACM International Joint Conference on Pervasive and Ubiquitous Computing, ACM, 2014, pp. 565–569.
[58] P.-A. Albinsson, S. Zhai, High precision touch screen interaction, in: Proceedings of the SIGCHI Conference on Human Factors in Computing Systems, ACM, 2003, pp. 105–112.
[59] I. Al-Naimi, C.B. Wong, Indoor human detection and tracking using advanced smart floor, in: Information and Communication Systems (ICICS), 2017 8th International Conference, IEEE, 2017, pp. 34–39.
[60] T. Starner, B. Leibe, D. Minnen, T. Westyn, A. Hurst, J. Weeks, The perceptive workbench: computer-vision-based gesture tracking, object tracking, and 3d reconstruction for augmented desks, Mach. Vis. Appl. 14 (1) (2003) 59–71.
[61] L. Precision, Capacitive Sensor Operation and Optimization, Tech Note. Jul.
[62] S. Pan, N. Wang, Y. Qian, I. Velibeyoglu, H.Y. Noh, P. Zhang, Indoor person identification through footstep induced structural vibration, in: Proceedings of the 16th International Workshop on Mobile Computing Systems and Applications, ACM, Santa Fe, NM, 2015, pp. 81–86.
[63] J.M. Sabatier, A.E. Ekimov, A review of human signatures in urban environments using seismic and acoustic methods, in: Technologies for Homeland Security, 2008 IEEE Conference, IEEE, 2008, pp. 215–220.
[64] A. Subramanian, K.G. Mehrotra, C.K. Mohan, P.K. Varshney, T. Damarla, Feature selection and occupancy classification using seismic sensors, in: International Conference on Industrial, Engineering and Other Applications of Applied Intelligent Systems, Springer, 2010, pp. 605–614.
[65] S. Pan, M. Mirshekari, P. Zhang, H.Y. Noh, Occupant traffic estimation through structural vibration sensing. SPIE Smart Structures and Materials+ Nondestructive Evaluation and Health Monitoring, International Society for Optics and Photonics, Las Vegas, NV, 2016, 980306–980306.
[66] C. DeLoney, Person Identification and Gender Recognition from Footstep Sound Using Modulation Analysis, Tech. rep., DRUM, 2008.
[67] J.T. Geiger, M. Kneißl, B.W. Schuller, G. Rigoll, Acoustic gait-based person identification using hidden markov models, in: Proceedings of the 2014 Workshop on Mapping Personality Traits Challenge and Workshop, ACM, 2014, pp. 25–30.
[68] M. Mirshekari, S. Pan, A. Bannis, Y.P.M. Lam, P. Zhang, H.Y. Noh, Step-level person localization through sparse sensing of structural vibration, in: Proceedings of the 14th International Conference on Information Processing in Sensor Networks, ACM, 2015, pp. 376–377.
[69] M. Mirshekari, P. Zhang, H.Y. Noh, Non-intrusive occupant localization using floor vibrations in dispersive structure: poster abstract, in: Proceedings of the 14th ACM Conference on Embedded Network Sensor Systems CD-ROM, ACM, 2016, pp. 378–379.
[70] M. Goel, B. Lee, M.T. Islam Aumi, S. Patel, G. Borriello, S. Hibino, B. Begole, Surfacelink: using inertial and acoustic sensing to enable multi-device interaction on a surface, in: Proceedings of the 32nd Annual ACM Conference on Human Factors in Computing Systems, ACM, New York, NY, USA, 2014, pp. 1387–1396.
[71] S. Xu, L. Zhang, P. Zhang, H.Y. Noh, An indirect traffic monitoring approach using building vibration sensing system: poster abstract, in: Proceedings of the 14th ACM Conference on Embedded Network Sensor Systems CD-ROM, ACM, Stanford, CA, 2016, pp. 374–375.
[72] J. Han, M. Harishankar, X. Wang, A.J. Chung, P. Tague, Convoy: physical context verification for vehicle platoon admission, in: 18th International Workshop on Mobile Computing Systems and Applications (HotMobile), ACM, Sonoma California, 2017, pp. 73–78.